Hydrogen bonding rather than cation bridging promotes graphene oxide attachment to lipid membranes in the presence of heavy metals

Huimin Li[a], Haodong Ji[a], Ruijie Zhang[a], Wei Zhang[b], Baozhu Pan[c], Wen Liu[a]; Weiling Sun[a,d,*]

[a] College of Environmental Sciences and Engineering, Peking University, The Key Laboratory of Water and Sediment Sciences, Ministry of Education, Beijing 100871, China

[b] Department of Plant, Soil and Microbial Sciences; Environmental Science, and Policy Program, Michigan State University, East Lansing, Michigan 48824, United States

[c] State Key Laboratory of Eco-hydraulic in Northwest Arid Region of China, Xi'an University of Technology, Xi'an 710048, Shaanxi, China

[d] State Key Laboratory of Plateau Ecology and Agriculture, Qinghai University, Xining 810016, China

[*]Corresponding author. E-mail: wlsun@pku.edu.cn (W.L. Sun)

Text S1. DFT calculation

All DFT calculations were performed using DMOL[3] code in Materials Studio (v7.0).[1] The finite-sized model of graphene oxide (4×5 carbon ring) containing carboxyl group and amino group was used to investigate the interactions between the SSLBs and metal ions. Cu(II) surrounded by four water molecules ($[Cu(H_2O)_4]^{2+}$) was employed as the form of Cu(II) in aqueous solution,[2] wherease Fe (III), Ni (II) and Cd (II) were hydrated in $[M(H_2O)_6]^{n+}$ forms.[3-5] Geometry optimization was performed using generalized gradient approximation (GGA) with Perdew, Burke and Enzerhof (PBE) functional.[6, 7] The double numeric polarization (DNP) basis set was used to describe atomic orbitals.[6, 8] Transition state (TS) method was chose for the DFT-D correction. The calclulations were porformed in spin unrestricted mode and using fomal spin as initial. Effective core potentials treatment[6] and medium quality were used. The convergence tolerance for optimization were 2×10^{-5} Ha (energy), 0.004 Ha/Å (Max. force), and 0.005 Å (Max. displacement). Thermal smearing was used and its value was set at 0.005 Ha. The conductor-like screening model (COSMO) using water solvent with dielectric constant of 75.84 was used to treat the solvation effects. During calculation, monitor bonding was activated in bond calculation dialog to enable the automatic recalculation of bonds.

The binding energies (E_{bd}) were calculated as follows:

$$E_{bd} = E_{AB} - E_A - E_B \quad \text{(S1)}$$

where E_{AB} is the total energy for the attachment of GO or the adsorption of metals to SSLBs, and E_A and E_B are the energies of adsorbent (SSLBs) and adsorbate (GO or metals), respectively. The more negative value of E_{bd} represents a stronger binding of GO or metal ions with the SSLBs.[2]

Text S2. Calculation of single bilayer adsorption of lipids

The theoretical single bilayer adsorption amount of lipid (A_l) was calculated using surface area of silica bead as follows:

$$A_l = m_l / m_s$$

$$m_l = 2S_s * M_l / (S_l * N_A)$$

$$S_s = 4\pi r^2$$

$$m_s = \rho * \frac{4}{3}\pi r^3$$

where A_l is the adsorption amount of lipid on silica bead surface (mg/g), m_l is the mass of bilayer lipid adsorbed on one silica bead (g), m_s is the mass of one silica bead (kg), S_s is the surface area of one silica bead (m^2), M_l is the molar mass of lipid (699 g/mol for DOTAP; 786 g/mol for DOPC; 801 g/mol for DOPS), S_l is the area of headgroup for lipid (6.8×10^{-19} m^2), N_A is the Avogadro constant (6.022×10^{23} /mol), ρ is the density of silica bead (2.65×10^3 kg/m^3), and r is the radius of silica bead (2.5×10^{-9} m).

Text S3. Adsorption of metals by GO

To further understand the interaction mechanisms of the binary systems, batch experiments were conducted to investigate the affinity of different metal ions with GO. Zeta potential of negatively GO (−29.9 mV) decreased as metal ions adsorbed on its surface. The zeta potential of GO-Fe(III) complex were −19.9 mV, followed by GO-Cu(II) (−22.2 mV), GO-Ni(II) (−24.7 mV) and GO-Cd(II) (−26.7 mV) (Fig. S9a). Moreover, the larger aggregation of GO (327–1650 nm) was formed in the presence of metals, compared with the size of GO without metals (Fig. S9b). The promotion effect of metals decreased as Fe(III) (1650 nm) > Cu(II) (390 nm) > Ni(II) (330 nm) > Cd(II) (327 nm) (Fig. S9b). The adsorption concentration of metal ions by GO (quantified by the decrease of metal concentration in solution) showed the order of Fe(III) (9.91μM) > Cu(II) (6.46 μM) > Ni(II) (4.10 μM) > Cd(II) (1.93 μM) (Fig. S9c). This is consistent with previous studies, which revealed that the adsorption affinity of GO to Cu(II) was higher than those to Ni(II) and Cd(II).[9-11] In addition, Fe(III) showed much stronger interaction with GO. Similarly, Yang et al. (2016)[12] also found that the aggregation of GO caused by trivalent cation was higher than divalent cations.

GO was abundant in various oxygen-containing groups, which could serve as potential adsorption sites for metals. Previous studies suggested carboxyl groups mainly contribute to metal adsorption,[7] as well as carbonyl group (C=O), hydroxyl group (-OH) and epoxy group (C-O-C).[6, 13, 14] DFT calculation was conducted to reveal the combination between metal ions and oxygen-containing functional groups

on the GO surface (Table S8). Results showed that the strongest binding energy was found in carboxyl group (−78.97 to −116.21 kcal/mol), confirming with previous studies.[6, 13-15] As for different heavy metals adsorbed by GO, the binding energy followed the same order of Fe(III) > Cu(II) > Ni(II) > Cd(II).

Text S4. XPS and FTIR analysis

The C 1s spectra were deconvoluted into four peaks at 284.8 eV, 286.8 eV, 287.9 eV and 288.8 eV, assigned to C-C, C-O, C=O and O-C=O, respectively.[16-19] The O 1s spectra were deconvoluted into three peaks at 531.7 eV, 532.5 eV and 533.2 eV assigned to O-C=O, C-O, and C-OH/P-O-C, respectively. The P 2p peak was at 133.6 eV.[16] The Cu 2p spectra were deconvoluted into three peaks at 934.5 eV, 954.3 eV and 944.1 eV, assigned to Cu $2p_{1/2}$, Cu $2p_{3/2}$ and Cu 2p satellite, respectively.[21-23] The results of the XPS analysis are summarized in Table S17. When comparing the spectra of the SSLB(0)-GO sample with that of the SSLB(0) sample, a shift of 0.3 eV was observed for C-O in the C 1s spectra (Fig. S11a), and a shift of 0.4 eV for all three peaks in the O 1s spectra (Fig. S11b), indicating the contribution of ester and phosphate groups in the SSLB(0) to hydrogen bonding with the hydroxyl group of GO. When comparing the spectra of the SSLB(0)-Cu(II) sample with that of the SSLB(0) sample, a shift of 0.2 eV was observed for all three peaks in the O 1s and P 2p spectra (Fig. S11b and S11c), suggesting the binding of Cu(II) onto ester and phosphate group of SSLB(0). When comparing the spectra of the GO-Cu(II) sample with that of the GO sample, a shift of 0.2 eV was observed for C-O in the C 1s spectra (Fig. S11a), suggesting the binding of Cu(II) onto the carboxyl group of GO. Meanwhile, no obvious Cu 2p peaks were observed in the GO, SSLB(0) and GO-SSLB(0) samples, demonstrating free of Cu. The Cu 2p peaks in the spectra of GO-Cu(II), SSLB(0)-Cu(II) and SSLB(0)-GO-Cu(II) samples proved the loading of Cu(II).

For the SSLB(0)-GO-Cu(II) sample, the C-O peak (287.0 eV) was the same with that of the GO-SSLB(0) sample, but shifted by 0.2 eV from that of the SSLB(0)-Cu(II) sample (Fig. S11a). Similarly, the C-OH/ P-O-C (533.5 eV) peak of the SSLB(0)-GO-Cu(II) sample was the same with that of the GO-SSLB(0) sample, but shifted by 0.2 eV from that of the SSLB(0)-Cu(II) sample (Fig. S11b). The similarity of the spectra of the SSLB(0)-GO-Cu(II) with that of the SSLB(0)-GO sample and its difference from the spectra of the SSLB(0)-Cu(II) sample for key functional groups associated with C-O and C-OH/ P-O-C (ester and phosphate groups) suggested that SSLB(0) prefers to binding with GO by hydrogen bonding rather than to Cu(II) via cation bridging in the SSLB(0)-GO-Cu(II). This also further confirmed the interaction mechanism revealed by the DFT calculation and batch experiments.

For FTIR spectra, the peak around 1050, 1369, 1618 and 1720 cm^{-1} were assigned to C-O, O-C=O, C=C and C=O.[16, 17, 24-26] The band centered at 771, 1016 and 1280 cm^{-1} were due to P-O-C and P=O from phosphate group in the SSLB(0) sample.[27, 28] The peak at 1397 cm^{-1} resulted from the C-N of amino groups in the SSLBs.[29] As shown in FTIR spectra (Fig. S11e), for the GO-SSLB(0) sample, hydrogen bonding was confirmed by the shift of the -OH bond of GO from 3345 cm^{-1} to 3359 cm^{-1} and the O-C=O /C=O bond of SSLB(0) from 1360/1727 cm^{-1} to 1353/1720 cm^{-1}. For the SSLB(0)-Cu(II) sample, the band at 1360 cm^{-1} (O-C=O) shifted to 1355 cm^{-1} was attributed to the binding of Cu(II) onto SSLB(0) through ester group. For the GO-Cu(II) sample, the band at 1369 cm^{-1} (O-C=O) for the GO

shifted to 1351 cm^{-1}, suggesting the binding between Cu (II) and carboxyl groups in GO. The FTIR spectra did not reveal any distinguishable difference between the SSLB(0)-GO-Cu(II), SSLB(0)-GO, and SSLB(0)-Cu(II) samples, and therefore could not be used to identify dominant binding mechanism for the ternary system.

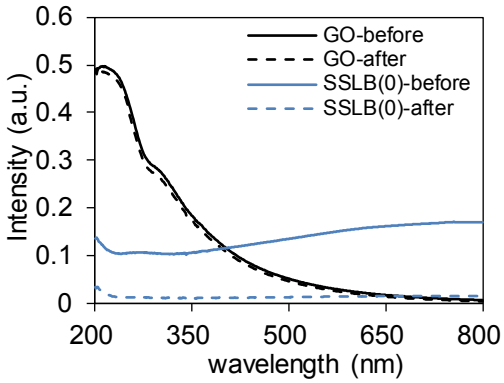

Fig. S1 UV-Vis absorbance of the GO and SSLB(0) suspensions before (solid line) and after (dash line) centrifugation at 2000 rpm for 5min.

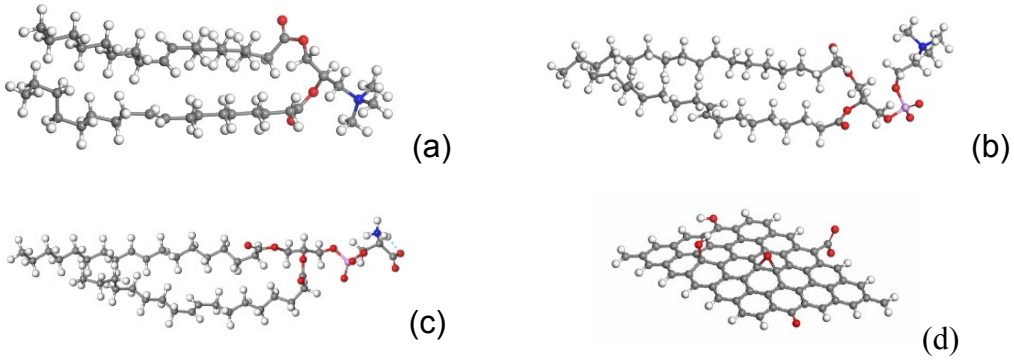

Fig. S2 Optimized structures of SSLB(+) (a), SSLB(0) (b), SSLB(-) (c) and GO (d).

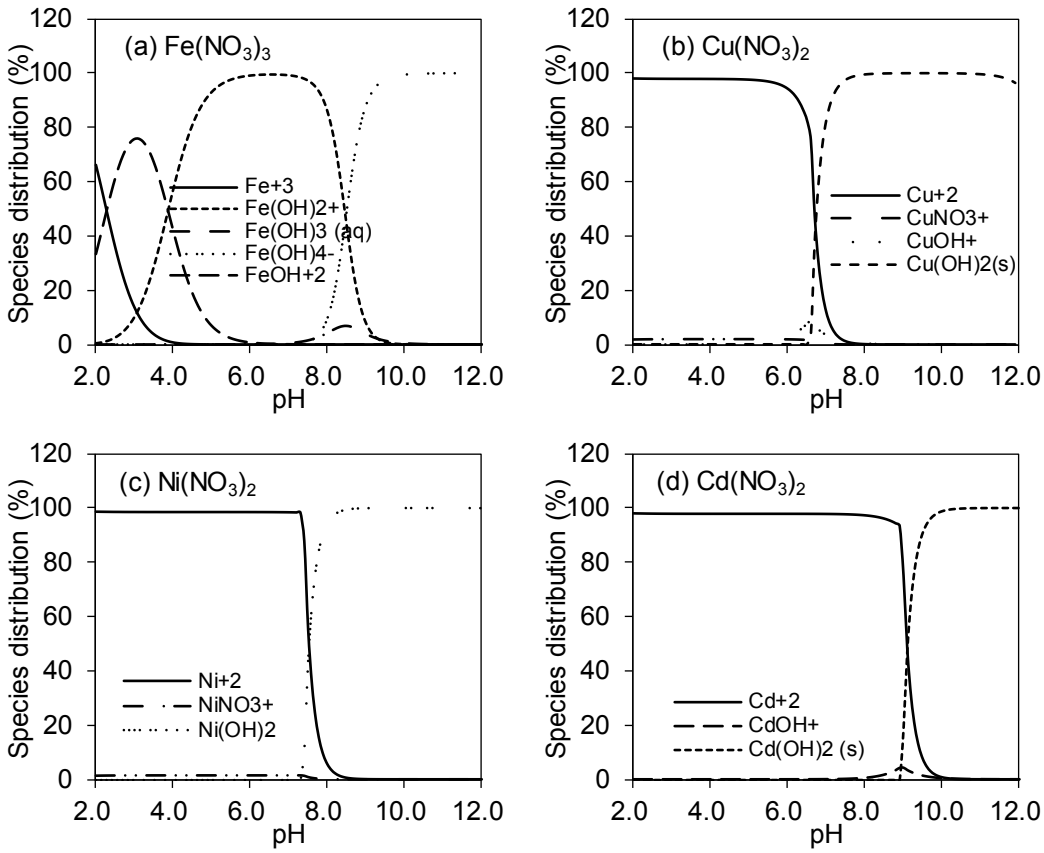

Fig. S3 Speciation distribution of heavy metals calculated using Visual MINTEQ version 3.0.

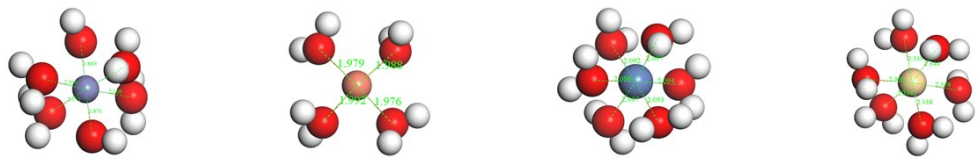

$Fe[(OH)_2(H_2O)_4]^+$ $Cu[(H_2O)_4]^{2+}$ $Ni[(H_2O)_6]^{2+}$ $Cd[(H_2O)_6]^{2+}$

Fig. S4 Optimized structures of hydrated heavy metals.

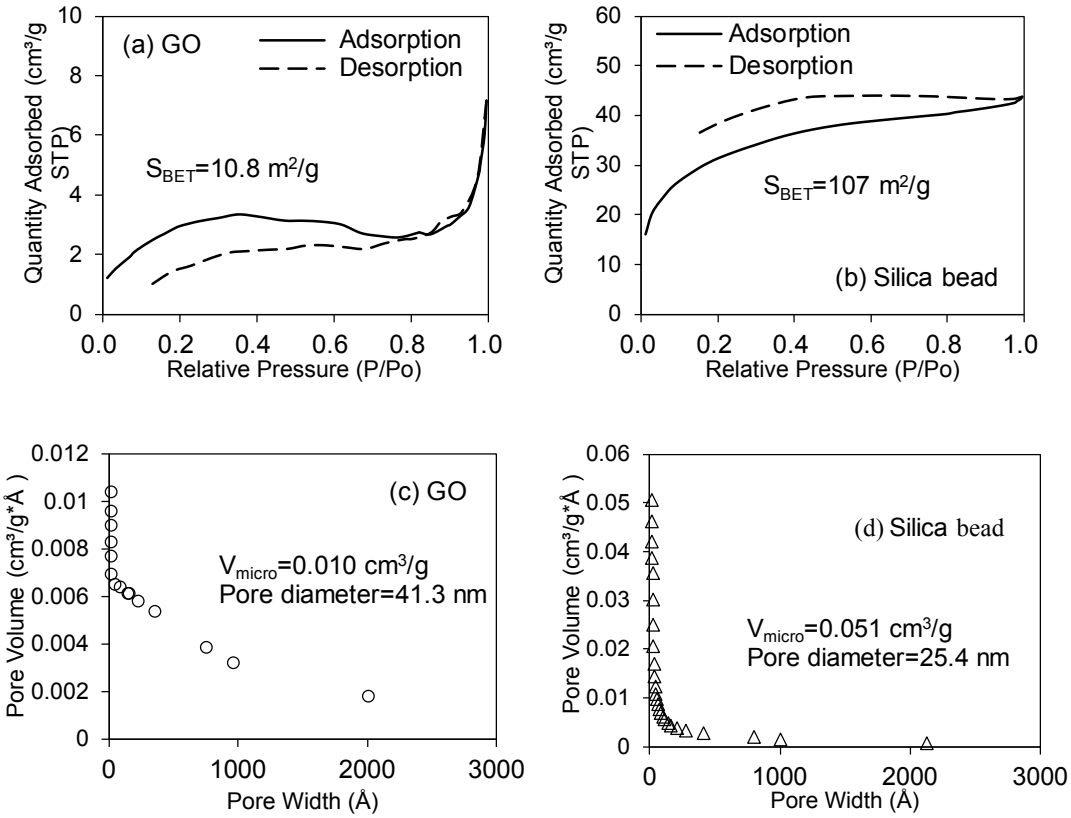

Fig. S5 Surface area and pore size distribution of GO and silica beads.

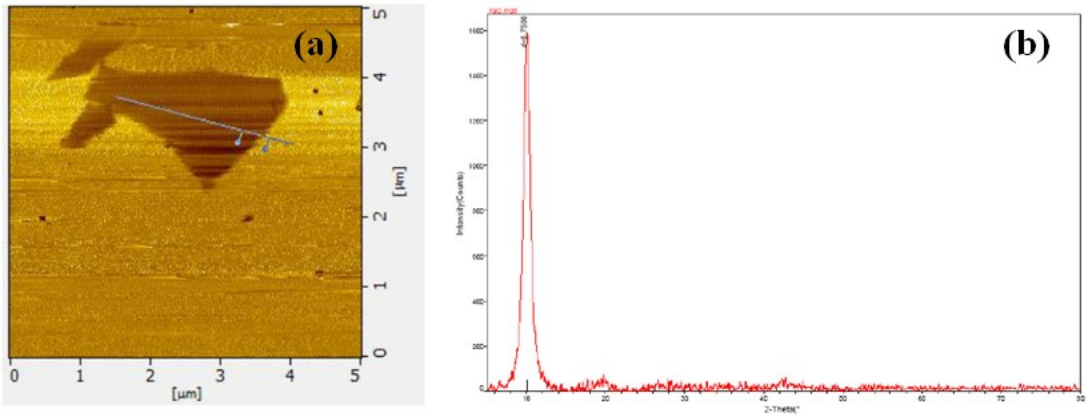

Fig. S6 AFM (a) and XRD (b) images of GO (obtained from the manufacturer).

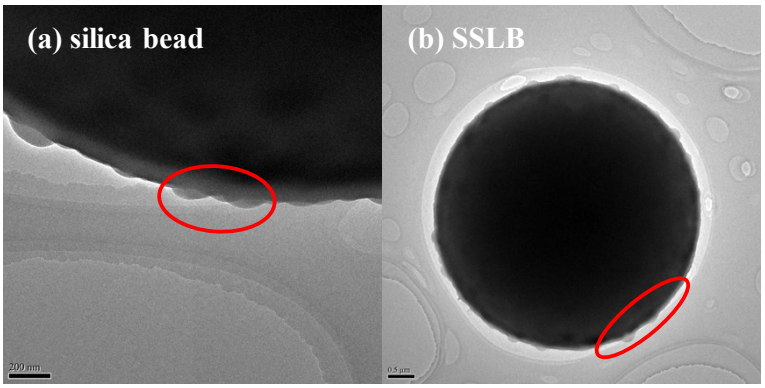

Fig. S7 TEM images of silica bead and SSLBs (rough silica surface protruding out of the lipid bilayer).

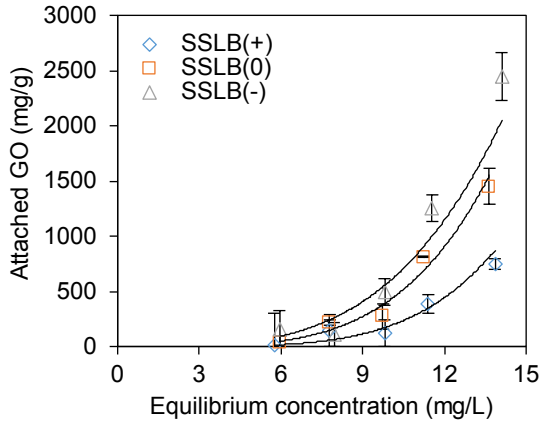

Fig.S8 The adsorption isotherms of GO onto SSLBs (the solid lines are the Freundlich model).

Adsorbent	Freundlich model ($Q = K_f \times C_e$)		
	K_f ((mg/g)/(mg/L)$^{1/n}$)	1/n	R^2
SSLB(+)	0.004	4.691	0.892
SSLB(0)	0.029	4.165	0.957
SSLB(-)	0.154	3.587	0.834

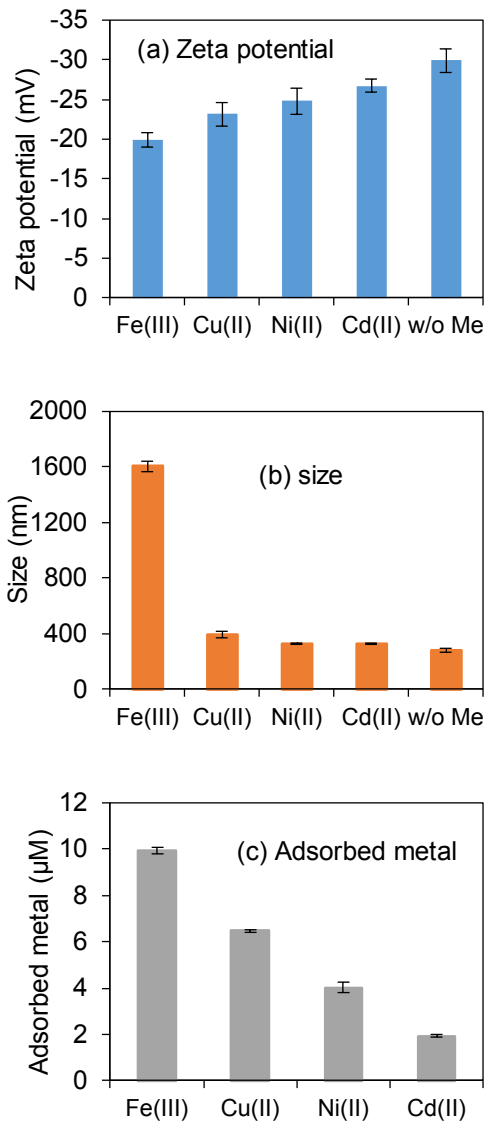

Fig. S9 Zeta potential (a) and size (b) of GO and the adsorbed metal by GO (c) (GO concentration of 10 mg/L, initial metal concentration of 10 μM, 0.01M $NaNO_3$).

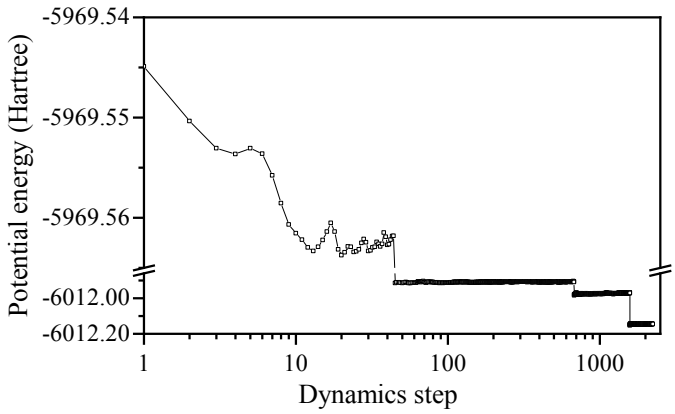
Potential energy (Hartree)
-5969.54
-5969.55
-5969.56
-6012.00
-6012.20
1
10
100
1000
Dynamics step

(a)

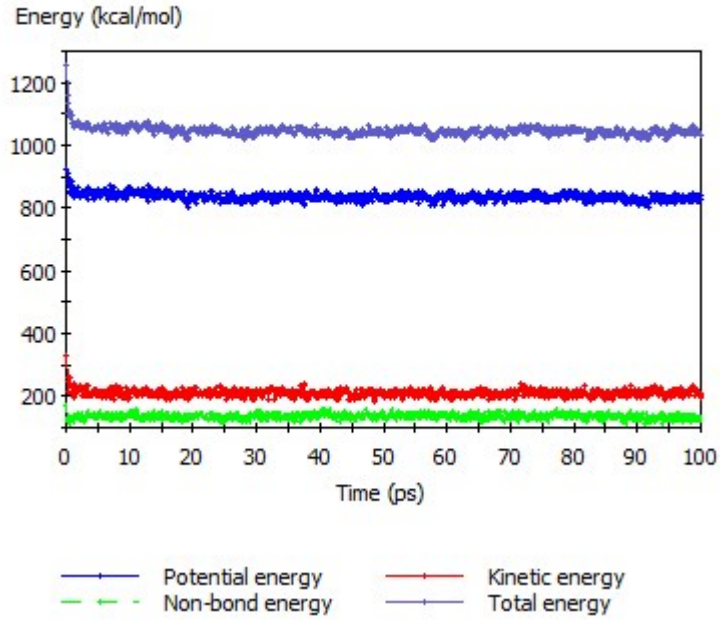
Energy (kcal/mol)
1200
1000
800
600
400
200
0
10
20
30
40
50
60
70
80
90
100
Time (ps)
Potential energy
Non-bond energy
Kinetic energy
Total energy

(b)

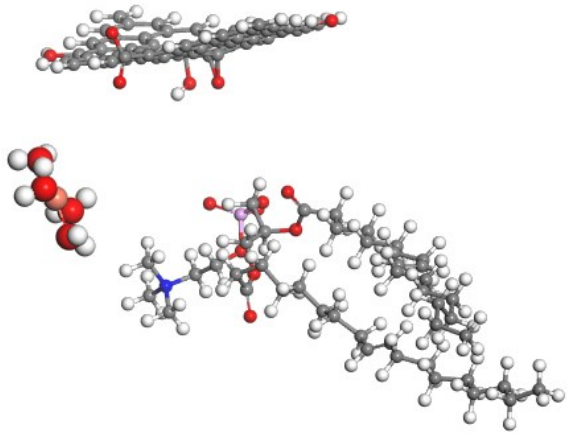

(c)

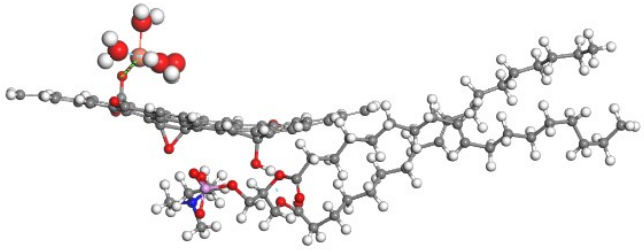

(d)

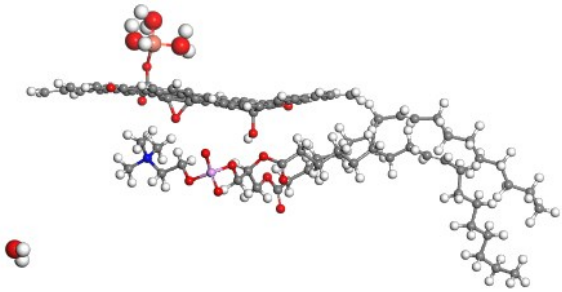

(e)

Fig. S10 Molecular dynamic simulation of the interactions between Cu(II), GO and SSLB(0) (Potential energies at different dynamic steps calculated using DMOL^3 code (a); Forcite dynamic energies at different simulation times (b); Snapshots of the initial state (c) and final states calculated by DMOL^3 (d) and Forcite modules (e).

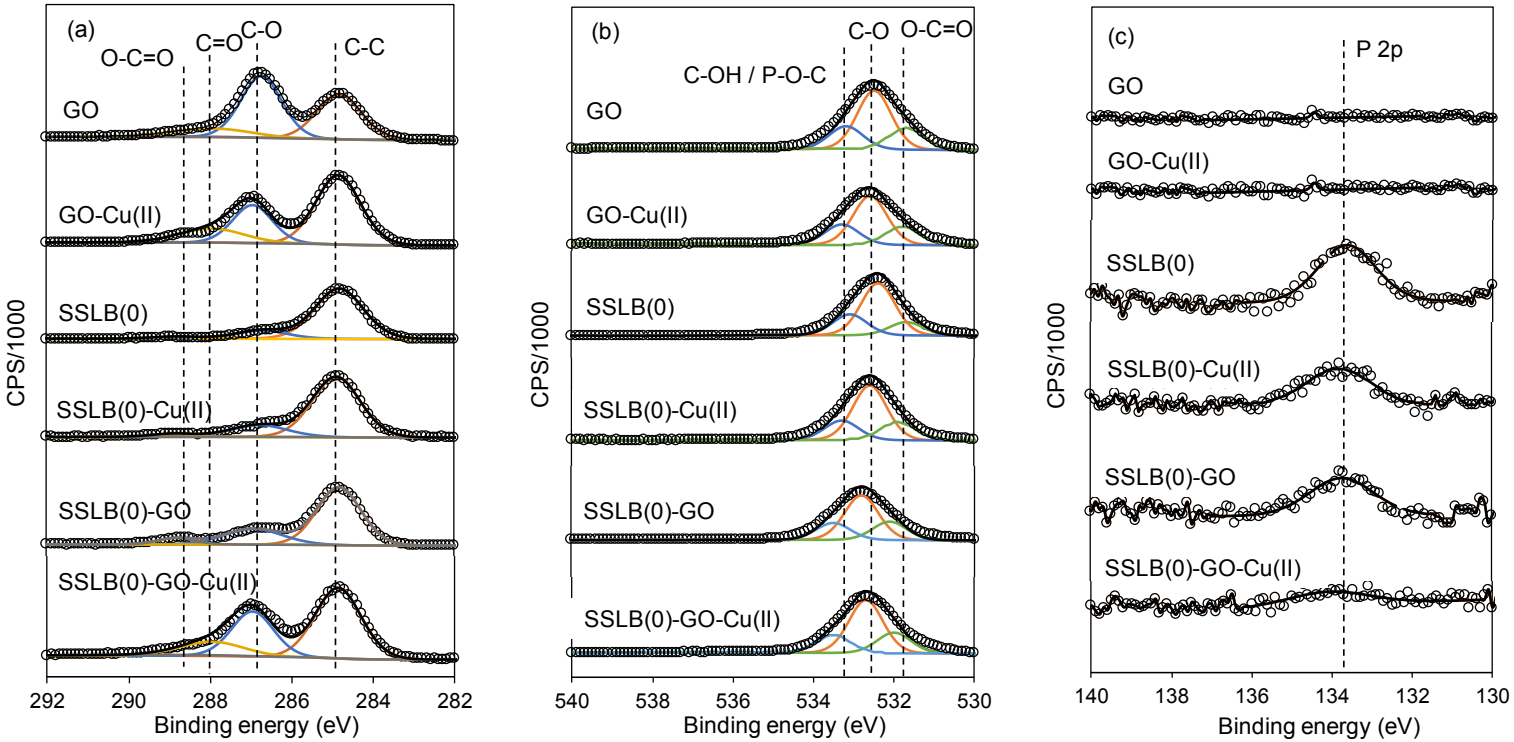
(a)
O-C=O
C=O
C-O
C-C
GO
GO-Cu(II)
SSLB(0)
SSLB(0)-Cu(II)
SSLB(0)-GO
SSLB(0)-GO-Cu(II)
CPS/1000
292
290
288
286
284
282
Binding energy (eV)
(b)
C-OH / P-O-C
C-O
O-C=O
GO
GO-Cu(II)
SSLB(0)
SSLB(0)-Cu(II)
SSLB(0)-GO
SSLB(0)-GO-Cu(II)
CPS/1000
540
538
536
534
532
530
Binding energy (eV)
(c)
P 2p
GO
GO-Cu(II)
SSLB(0)
SSLB(0)-Cu(II)
SSLB(0)-GO
SSLB(0)-GO-Cu(II)
CPS/1000
140
138
136
134
132
130
Binding energy (eV)

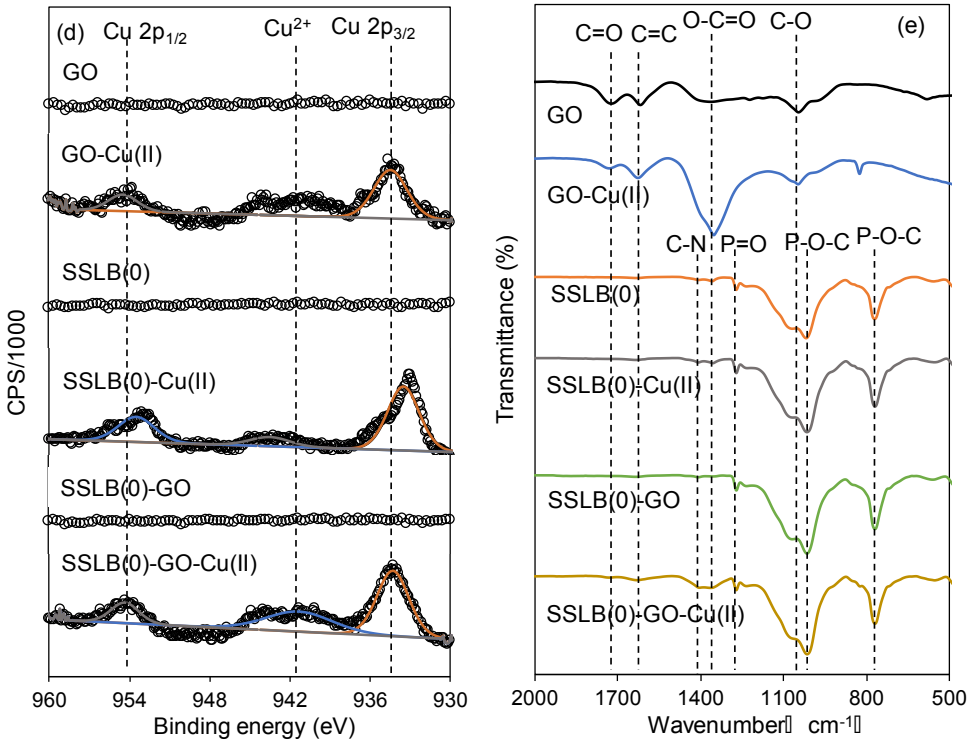

Fig. S11 High resolution XPS C1s (a), O 1s (b), P 2p (c), Cu 2p (d) and FTIR (e) spectra of GO, GO-Cu(II), SSLB(0), SSLB(0)-Cu(II), SSLB(0)-GO and SSLB(0)-GO-Cu(II).

Table S1 DFT calculation results for the adsorption of GO by SSLB(+).

Binding group in SSLB(+)		Total energy (*E*, Hartree)			Binding group in SSLB(+)	Total energy (*E*, Hartree)	Binding site
		SSLB(+)	GO	SSLB(+)			
Ester group	E1	-2002.246	-2786.415	-4788.678	-10.65	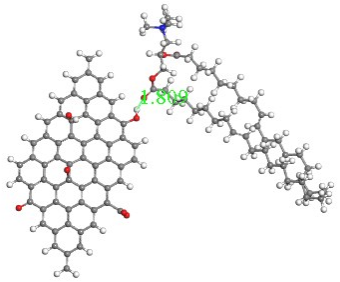	Hydrogen bonding between C=O of −COO− in SSLB(+) and −OH on the edge of GO
	E2	-2002.246	-2786.415	-4788.680	-12.17	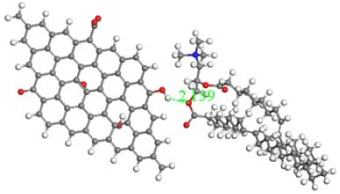	Hydrogen bonding between C−O of −COO− in SSLB(+) and −OH on the edge of GO
	E3	-2002.246	-2786.415	-4788.693	-19.89	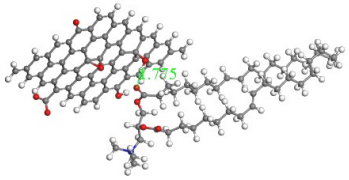	Hydrogen bonding between C=O of −COO− in SSLB(+) and −OH on the basal plane of GO

Binding group in SSLB(+)	Total energy (*E*, Hartree)			Binding group in SSLB(+)	Total energy (*E*, Hartree)	Binding site
	SSLB(+)	GO	SSLB(+)			
E4	-2002.246	-2786.415	-4788.703	-26.21	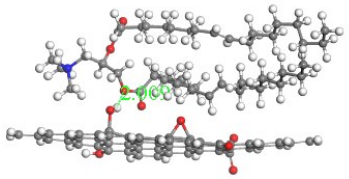	Hydrogen bonding between C−O of −COO− in SSLB(+) and −OH on the basal plane of GO

Table S2 DFT calculation results for the adsorption of GO by SSLB(0).

Binding group in SSLB(0)		Total energy (*E*, Hartree)			Binding energy (kcal/mol)	Structure (bond length, Å)	Binding site
		SSLB(0)	GO	GO-SSLB(0)			
Ester group	E1	-2723.099	-2786.415	-5509.607	-58.25	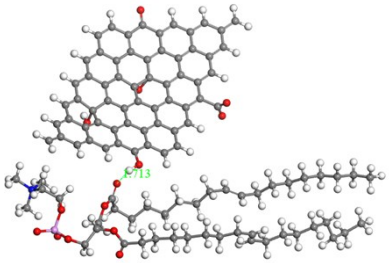	Hydrogen bonding between C=O of −COO− in SSLB(0) and −OH on the edge of GO
	E2	-2723.099	-2786.415	-5509.601	-54.26	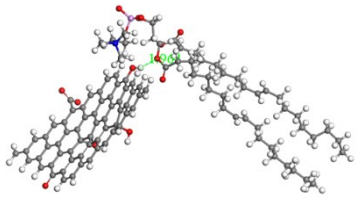	Hydrogen bonding between C−O of −COO− in SSLB(0) and −OH on the edge of GO
	E3	-2723.099	-2786.415	-5509.613	-62.04	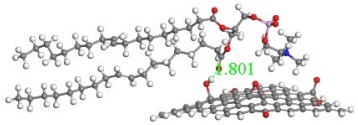	Hydrogen bonding between C=O of −COO− in SSLB(0) and −OH on the basal plane of GO
	E4	-2723.099	-2786.415	-5509.615	-62.90	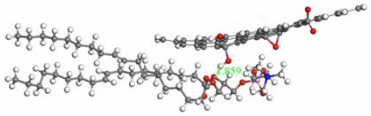	Hydrogen bonding between C−O of −COO− in SSLB(0) and −OH on

Binding group in SSLB(0)		Total energy (*E*, Hartree)			Binding energy (kcal/mol)	Structure (bond length, Å)	Binding site
		SSLB(0)	GO	GO-SSLB(0)			
							the basal plane of GO
Phosphate group	P1	-2723.099	-2786.415	-5509.602	-54.90	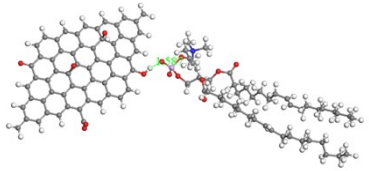	Hydrogen bonding between P-O of $–PO_4^-$ and −OH on the edge of GO
	P2	-2723.099	-2786.415	-5509.598	-52.52	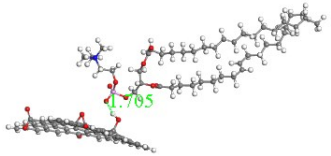	Hydrogen bonding between P-O of $–PO_4^-$ and −OH on the basal plane of GO
	P3	-2723.099	-2786.415	-5509.601	-54.19	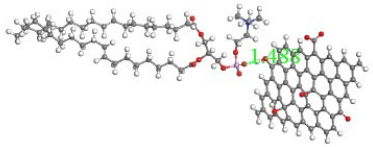	Hydrogen bonding between P=O of $–PO_4^-$ and −OH on the edge of GO
	P4	-2723.099	-2786.415	-5509.606	-57.69	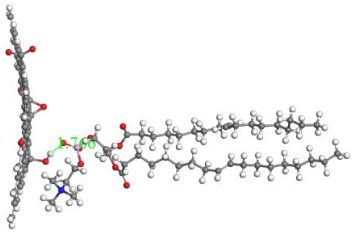	Hydrogen bonding between P=O of $–PO_4^-$ and −OH on the basal plane of GO

Table S3 DFT calculation results for the adsorption of GO by SSLB(−).

Binding group in SSLB(−)		Total energy (*E*, Hartree)			Binding energy (kcal/mol)	Structure (bond length, Å)	Binding site
		SSLB(−)	GO	GO-SSLB(−)			
Amino group	A1	-2793.321	-2786.415	-5579.842	-66.43	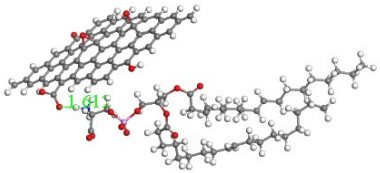	Hydrogen bonding between $-NH_3$ and C−O in $-COO^-$ of GO
	A2	-2793.321	-2786.415	-5579.830	-58.54	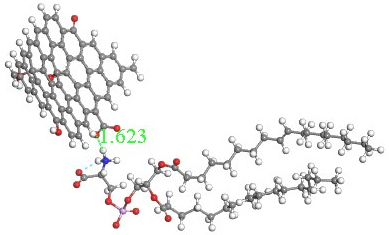	Hydrogen bonding between $-NH_3$ and C=O in $-COO^-$ of GO
	A3	-2793.321	-2786.415	-5579.813	-48.31	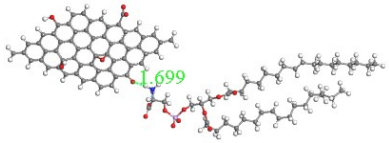	Hydrogen bonding between $-NH_3$ and C=O of GO
	A4	-2793.321	-2786.415	-5579.813	-48.16	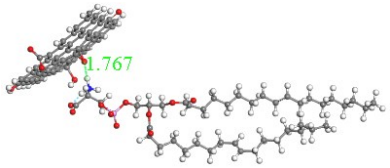	Hydrogen bonding between $-NH_3$ and C−O−C of GO

Binding group in SSLB(−)		Total energy (E, Hartree)			Binding energy (kcal/mol)	Structure (bond length, Å)	Binding site
		SSLB(−)	GO	GO-SSLB(−)			
	A5	-2793.321	-2786.415	-5579.803	-41.95	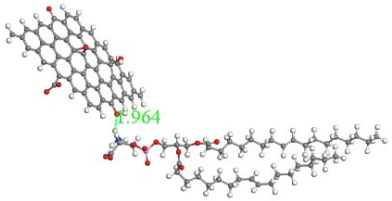	Hydrogen bonding between $-NH_3$ and −OH on the edge of GO
	A6	-2793.321	-2786.415	-5579.815	-49.70	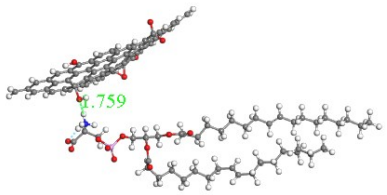	Hydrogen bonding between $-NH_3$ and −OH on the basal plane of GO
Ester group	E1	-2793.321	-2786.415	-5579.838	-64.15	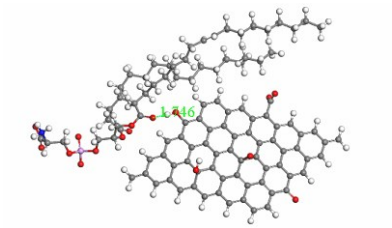	Hydrogen bonding between C=O of −COO− in SSLB(-) and −OH on the edge of GO

Binding group in SSLB(−)		Total energy (*E*, Hartree)			Binding energy (kcal/mol)	Structure (bond length, Å)	Binding site
		SSLB(−)	GO	GO-SSLB(−)			
	E2	-2793.321	-2786.415	-2786.415258	-54.71	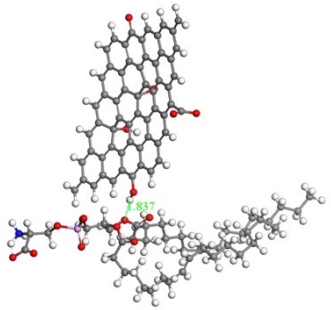	Hydrogen bonding between C−O of −COO− in SSLB(-) and −OH on the edge of GO
	E3	-2793.321	-2786.415	-5579.841	-65.67	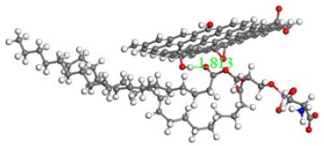	Hydrogen bonding between C=O of −COO− in SSLB(-) and −OH on the basal plane of GO
	E4	-2793.321	-2786.415	-5579.840	-65.36	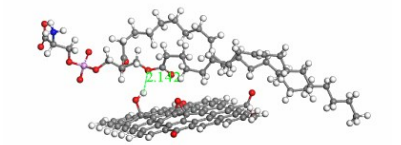	Hydrogen bonding between C−O of −COO− in SSLB(-) and −OH on the basal plane of GO
Carboxyl group	C1	-2793.321	-2786.415	-5579.816	-49.94	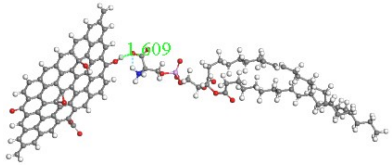	Hydrogen bonding between C−O of –COO⁻ in SSLB(-) and−OH on the edge of GO

Binding group in SSLB(−)		Total energy (*E*, Hartree)			Binding energy (kcal/mol)	Structure (bond length, Å)	Binding site
		SSLB(−)	GO	GO-SSLB(−)			
	C2	-2793.321	-2786.415	-5579.821	-53.25	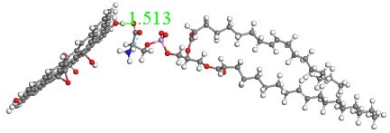	Hydrogen bonding between C=O of $-COO^-$ in SSLB(-) and −OH on the edge of GO
	C3	-2793.321	-2786.415	-5579.814	-48.77	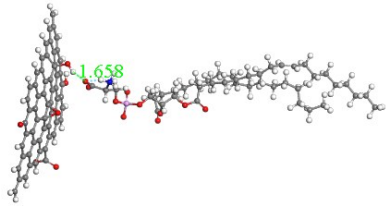	Hydrogen bonding between C−O of $-COO^-$ in SSLB(-) and −OH on the basal plane of GO
	C4	-2793.321	-2786.415	-5579.813	-48.43	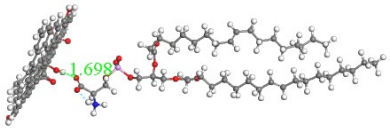	Hydrogen bonding between C=O of $-COO^-$ in SSLB(-) and −OH on the basal plane of GO
Phosphate group	P1	-2793.321	-2786.415	-5579.822	-54.10	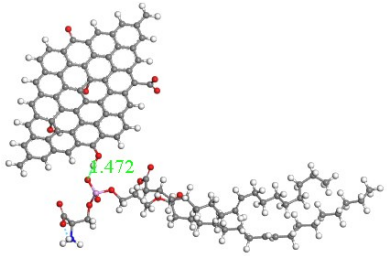	Hydrogen bonding between P-O of $-PO_4^-$ and −OH on the edge of GO

Binding group in SSLB(−)	Total energy (*E*, Hartree)			Binding energy (kcal/mol)	Structure (bond length, Å)	Binding site
	SSLB(−)	GO	GO-SSLB(−)			
P2	-2793.321	-2786.415	-5579.826	-56.07	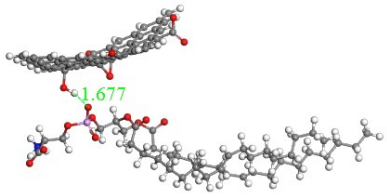	Hydrogen bonding between P-O of $–PO_4^-$ and −OH on the basal plane of GO
P3	-2793.321	-2786.415	-5579.828	-57.65	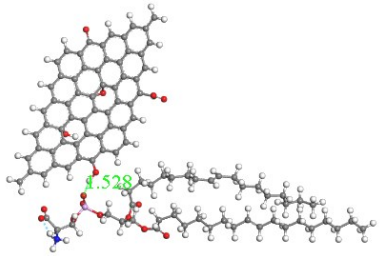	Hydrogen bonding between P=O of $–PO_4^-$ and −OH on the edge of GO
P4	-2793.321	-2786.415	-5579.840	-64.98	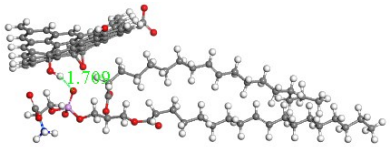	Hydrogen bonding between P=O of $–PO_4^-$ and −OH on the basal plane of GO

Table S4 Physicochemical properties of the studied metals[30-34]

	N	PE	Charge	R_I (Å)	R_H (Å)	logK_{H2O}	Charge/R_I
Fe (III)	6	1.83	+3	0.75	4.57	-2.19	4.00
Cu (II)	4	1.90	+2	0.72	4.19	-7.50	2.78
Ni (II)	6	1.91	+2	0.83	4.04	-9.90	2.41
Cd (II)	6	1.69	+2	0.97	4.26	-10.10	2.06

N: number of waters of hydration

PE: Pauling electronegativity

R_I: ionic radius

R_H: hydrated radius

LogK_{H2O}: log of the fist hydrolysis constant

Table S5 DFT calculation results for the adsorption of metals by SSLB(+).

Binding group	Total energy (*E*, Hartree)				Binding energy (kcal/mol)	Structure (bond length, Å)
	Metal	SSLB(+)	Metal-SSLB (+)			
Ester group	Fe(III)	-581.037	-2002.246	-2583.404	-76.19	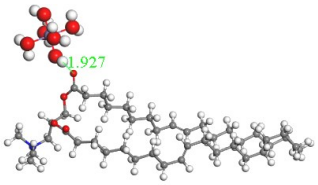
	Cu(II)	-502.678	-2002.246	-2505.028	-65.23	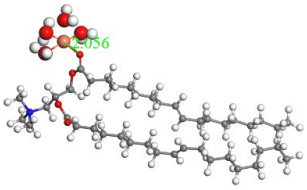
	Ni(II)	-629.160	-2002.246	-2631.498	-57.81	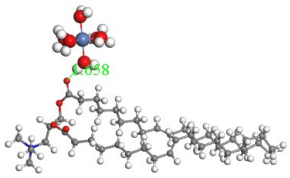
	Cd(II)	-625.890	-2002.246	-2628.222	-54.10	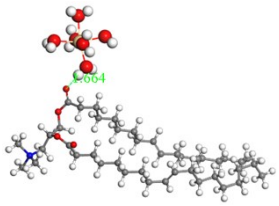

Table S6 DFT calculation results for the adsorption of metals by SSLB(0).

Binding site		Total energy (*E*, Hartree)			Binding energy (kcal/mol)	Structure (bond length, Å)
		Metal	SSLB(0)	Metal-SSLB (0)		
Phosphate group	Fe(III)	-581.037	-2723.099	-3304.231	-59.85	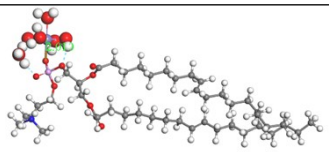
	Cu(II)	-502.678	-2723.099	-3225.852	-46.77	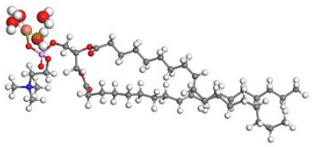
	Ni(II)	-629.160	-2723.099	-3352.328	-43.19	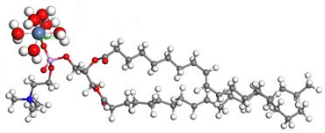
	Cd(II)	-625.890	-2723.099	-3349.051	-39.07	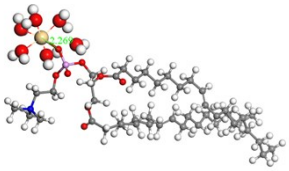
Ester group	Fe(III)	-581.037	-2723.099	-3304.195	-37.16	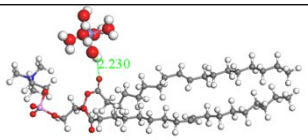
	Cu(II)	-502.678	-2723.099	-3225.823	-28.85	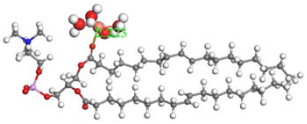
	Ni(II)	-629.160	-2723.099	-3352.299	-25.38	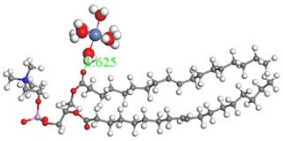
	Cd(II)	-625.890	-2723.099	-3349.027	-23.93	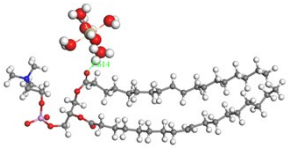

Table S7 DFT calculation results for the adsorption of metals by SSLB(−).

Binding site	Total energy (*E*, Hartree)				Binding energy (kcal/mol)	Structure (bond length, Å)
	Metal	SSLB(−)	Metal-SSLB (−)			
Carboxyl group	Fe(III)	-581.037	-2793.321	-3374.461	-64.88	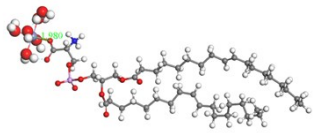
	Cu(II)	-502.678	-2793.321	-3296.075	-47.69	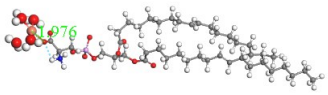
	Ni(II)	-629.160	-2793.321	-3422.540	-37.02	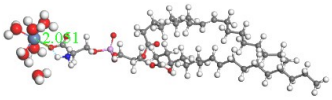
	Cd(II)	-625.890	-2793.321	-3419.268	-35.77	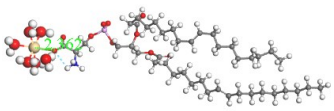
Phosphate group	Fe(III)	-581.037	-2793.321	-3374.462	-65.55	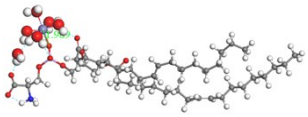
	Cu(II)	-502.678	-2793.321	-3296.088	-55.56	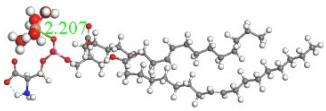
	Ni(II)	-629.160	-2793.321	-3422.563	-51.67	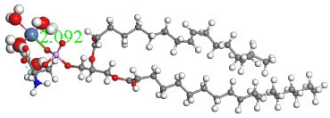
	Cd(II)	-625.890	-2793.321	-3419.284	-45.72	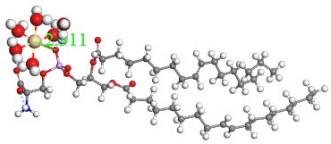
Ester group	Fe(III)	-581.037	-2793.321	-3374.449	-57.44	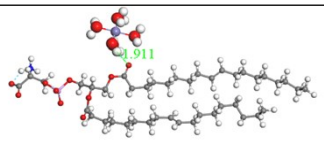
	Cu(II)	-502.678	-2793.321	-3296.046	-29.49	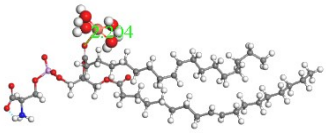

Binding site	Total energy (*E*, Hartree)				Binding energy (kcal/mol)	Structure (bond length, Å)
		Metal	SSLB(−)	Metal-SSLB (−)		
	Ni(II)	-629.160	-2793.321	-3422.519	-29.06	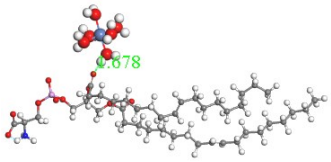
	Cd(II)	-625.890	-2793.321	-3419.248	-23.22	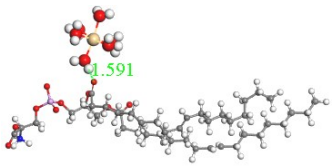
Amino group	Fe(III)	-581.037	-2793.321	-3374.442	-52.68	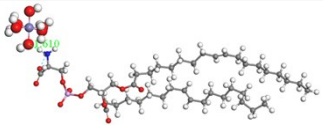
	Cu(II)	-502.678	-2793.321	-3296.030	-19.41	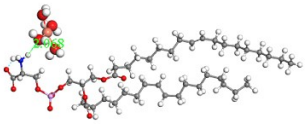
	Ni(II)	-629.160	-2793.321	-3422.510	-18.11	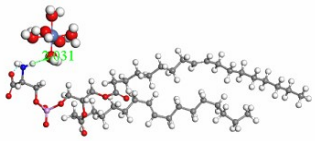
	Cd(II)	-625.890	-2793.321	-3419.240	-17.84	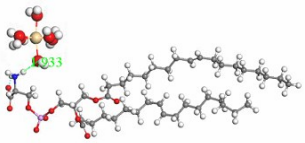

Table S8 DFT calculation results for the adsorption of metals by GO.

Binding group	Total energy (*E*, Hartree)				Binding energy (kcal/mol)	Structure (bond length, Å)
	Metal	GO	Metal-GO			
-COO$^-$	Fe(III)	-581.037	-2786.415	-3367.637	-116.21	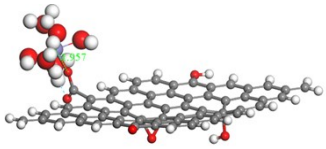
	Cu(II)	-502.678	-2786.415	-3289.259	-103.76	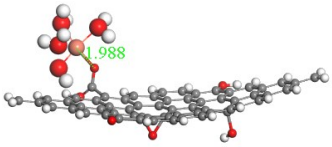
	Ni(II)	-629.160	-2786.415	-3415.724	-93.48	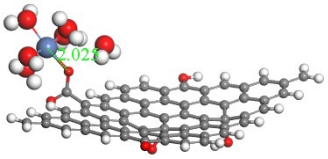
	Cd(II)	-625.890	-2786.415	-3412.431	-78.97	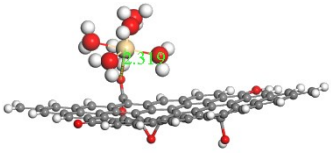
-C=O	Fe(III)	-581.037	-2786.415	-3367.622	-106.39	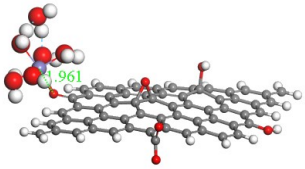
	Cu(II)	-502.678	-2786.415	-3289.245	-95.14	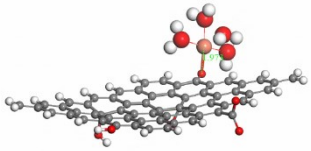
	Ni(II)	-629.160	-2786.415	-3415.701	-79.22	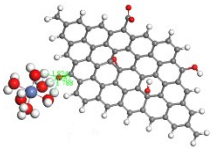
	Cd(II)	-625.890	-2786.415	-3412.422	-73.75	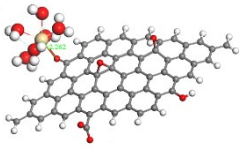
C-O-C	Fe(III)	-581.037	-2786.415	-3367.618	-104.18	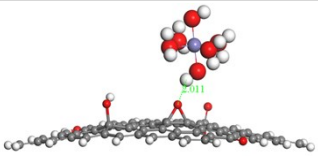

Binding group	Total energy (*E*, Hartree)				Binding energy (kcal/mol)	Structure (bond length, Å)
		Metal	GO	Metal-GO		
	Cu(II)	-502.678	-2786.415	-3289.242	-93.39	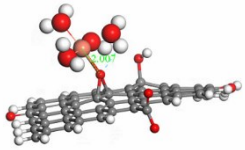
	Ni(II)	-629.160	-2786.415	-3415.724	-93.62	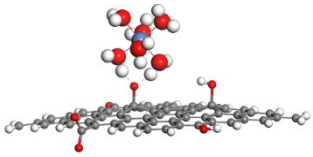
	Cd(II)	-625.890	-2786.415	-3412.422	-73.79	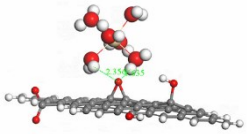
	Fe(III)	-581.037	-2786.415	-3367.601	-93.20	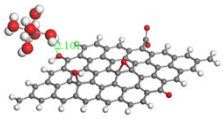
C-OH (edge)	Cu(II)	-502.678	-2786.415	-3289.225	-82.52	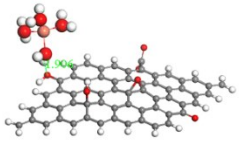
	Ni(II)	-629.160	-2786.415	-3415.687	-70.17	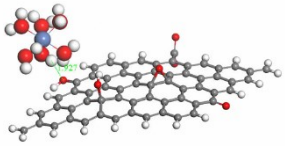
	Cd(II)	-625.890	-2786.415	-3412.409	-65.32	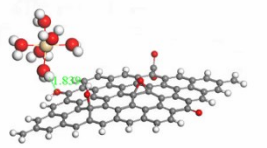
	Fe(III)	-581.037	-2786.415	-3367.614	-101.66	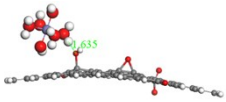
C-OH (basal plane)	Cu(II)	-502.678	-2786.415	-3289.233	-87.76	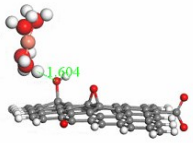
	Ni(II)	-629.160	-2786.415	-3415.696	-75.94	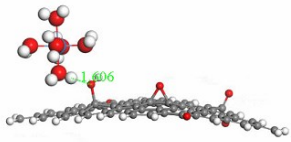

Binding group	Total energy (*E*, Hartree)			Binding energy (kcal/mol)	Structure (bond length, Å)
	Metal	GO	Metal-GO		
	Cd(II)	-625.890	-2786.415	-3412.422	-73.25	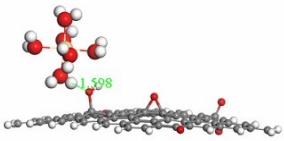

Table S9 DFT calculation results for the adsorption of GO-metal by SSLB(+).

Binding way	Total energy (*E*, Hartree)			Binding energy	Structure	Binding site
	GO-Metal	SSLBs	SSLB-GO-metal	(kcal/mol)	(bond length, Å)	
SSLB(+)–[GO-Fe]	-3367.637	-2002.246	-5370.160	-173.74	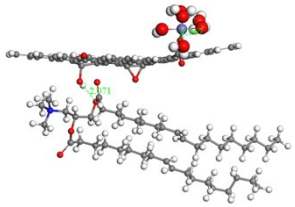	Hydrogen bonding between C−O of −COO− in SSLB(+) and −OH on the basal plane of GO
SSLB(+)–[GO-Cu]	-3289.259	-2002.246	-5291.750	-154.45	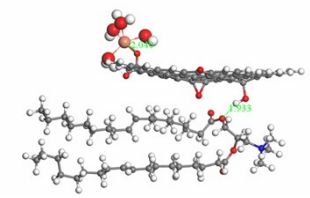	Hydrogen bonding between C−O of −COO− in SSLB(+) and −OH on the basal plane of GO
SSLB(+)–[GO-Ni]	-3415.724	-2002.246	-5418.211	-151.43	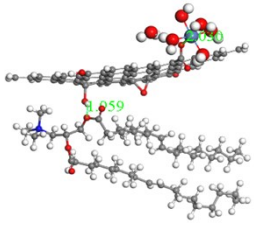	Hydrogen bonding between C−O of −COO− in SSLB(+) and −OH on the basal plane of GO

Binding way	Total energy (*E*, Hartree)			Binding energy	Structure	Binding site
	GO-Metal	SSLBs	SSLB-GO-metal	(kcal/mol)	(bond length, Å)	
SSLB(+)–[GO-Cd]	-3412.431	-2002.246	-5414.917	-151.12	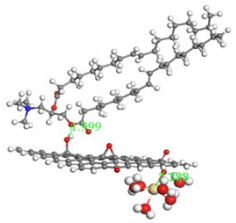	Hydrogen bonding between C−O of −COO− in SSLB(+) and −OH on the basal plane of GO
[GO-Fe]–SSLB(+)	-3367.637	-2002.246	-5370.152	-168.59	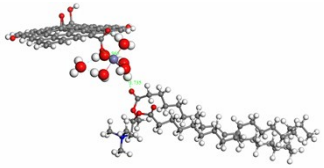	Coordination between Fe(III) and C−O in −COO− of SSLB(+)
[GO-Cu]–SSLB(+)	-3289.259	-2002.246	-5291.740	-147.94	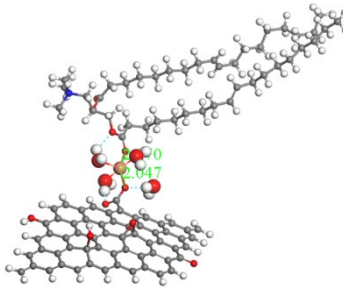	Coordination between Cu(II) and C−O in −COO− of SSLB(+)

Binding way	Total energy (*E*, Hartree)			Binding energy	Structure	Binding site
	GO-Metal	SSLBs	SSLB-GO-metal	(kcal/mol)	(bond length, Å)	
[GO-Ni]–SSLB(+)	-3415.724	-2002.246	-5418.200	-144.57	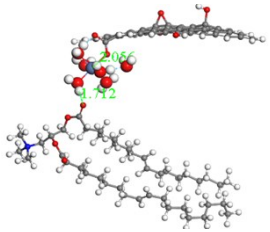	Coordination between Ni(II) and C−O in −COO− of SSLB(+)
[GO-Cd]–SSLB(+)	-3412.431	-2002.246	-5414.900	-140.30	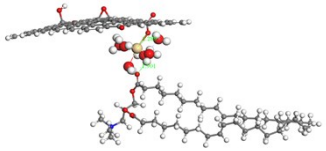	Coordination between Cd(II) and C−O in −COO− of SSLB(+)

Table S10 DFT calculation results for the adsorption of GO-metal by SSLB(0).

Binding mode	Total energy (*E*, Hartree)			Binding energy	Structure	Binding site
	GO-Metal	SSLBs	SSLB-GO-metal	(kcal/mol)	(bond length, Å)	
SSLB(0)–[GO-Fe]	-3367.637	-2723.099	-6090.962	-141.56	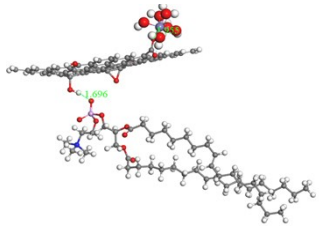	Hydrogen bonding between C−O of −COO− in SSLB(0) and −OH on the basal plane of GO
SSLB(0)–[GO-Cu]	-3289.259	-2723.099	-6012.570	-133.25	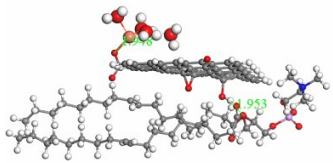	Hydrogen bonding between C−O of −COO− in SSLB(0) and −OH on the basal plane of GO
SSLB(0)–[GO-Ni]	-3415.724	-2723.099	-6139.032	-131.44	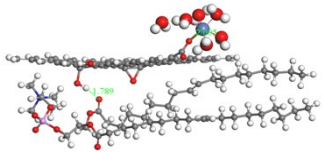	Hydrogen bonding between C−O of −COO− in SSLB(0) and −OH on the basal plane of GO
SSLB(0)–[GO-Cd]	-3412.431	-2723.099	-6135.734	-127.89	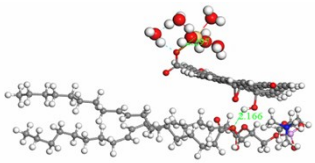	Hydrogen bonding between C−O of −COO− in SSLB(0) and −OH on the basal plane of GO

Binding mode	Total energy (*E*, Hartree)			Binding energy	Structure	Binding site
	GO-Metal	SSLBs	SSLB-GO-metal	(kcal/mol)	(bond length, Å)	
[GO-Fe]–SSLB(0)	-3367.637	-2723.099	-6090.957	-138.44	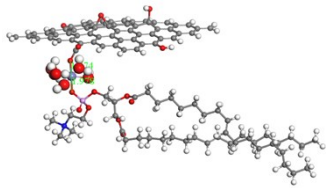	Coordination between Fe(III) and P-O in $–PO_4^-$ of SSLB(0)
[GO-Cu]–SSLB(0)	-3289.259	-2723.099	-6012.567	-131.17	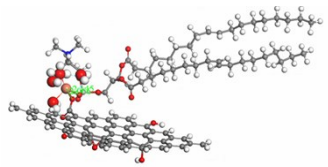	Coordination between Cu(II) and P-O in $–PO_4^-$ of SSLB(0)
[GO-Ni]–SSLB(0)	-3415.724	-2723.099	-6139.022	-124.89	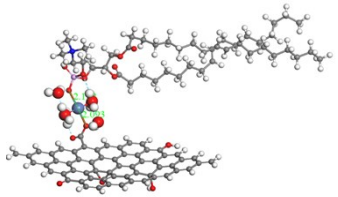	Coordination between Ni(II) and P-O in $–PO_4^-$ of SSLB(0)
[GO-Cd]–SSLB(0)	-3412.431	-2723.099	-6135.729	-124.82	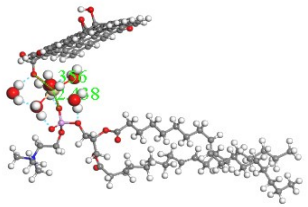	Coordination between Cd(II) and P-O in $–PO_4^-$ of SSLB(0)

Table S11 DFT calculation results for the adsorption of GO-metal by SSLB(−).

Binding mode	Total energy (*E*, Hartree)			Binding energy	Structure	Binding site
	GO-Metal	SSLBs	SSLB-GO-metal	(kcal/mol)	(bond length, Å)	
SSLB(-)–[GO-Fe]	-3367.637	-2793.321	-6161.232	-171.77	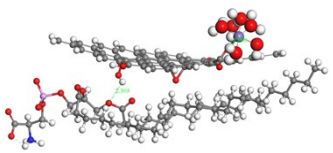	Hydrogen bonding between C=O of −COO− in SSLB(-) and −OH on the basal plane of GO
SSLB(-)–[GO-Cu]	-3289.259	-2793.321	-6082.815	-147.97	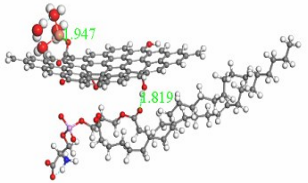	Hydrogen bonding between C=O of −COO− in SSLB(-) and −OH on the basal plane of GO
SSLB(-)–[GO-Ni]	-3415.724	-2793.321	-6209.273	-143.04	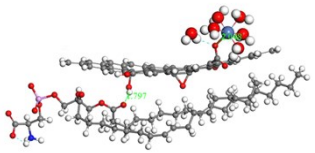	Hydrogen bonding between C=O of −COO− in SSLB(-) and −OH on the basal plane of GO
SSLB(-)–[GO-Cd]	-3412.431	-2793.321	-6205.973	-139.17	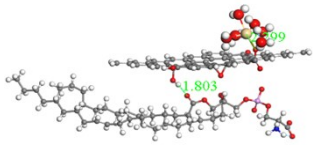	Hydrogen bonding between of C=O of −COO− in SSLB(-) and −OH on the basal plane of GO

Binding mode	Total energy (*E*, Hartree)			Binding energy	Structure	Binding site
	GO-Metal	SSLBs	SSLB-GO-metal	(kcal/mol)	(bond length, Å)	
[GO-Fe]–SSLB(-)	-3367.637	-2793.321	-6161.202	-153.14	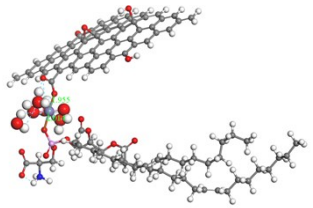	Coordination between Fe(III) and P-O in $–PO_4^-$ of SSLB(-)
[GO-Cu]–SSLB(-)	-3289.259	-2793.321	-6082.805	-141.70	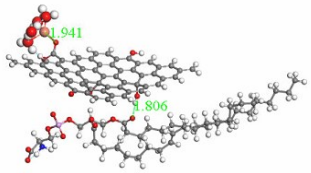	Coordination between Cu(II) and P-O in $–PO_4^-$ of SSLB(-)
[GO-Ni]–SSLB(-)	-3415.724	-2793.321	-6209.2 6	-131.98	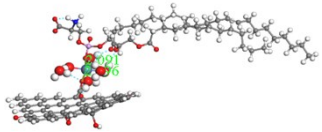	Coordination between Ni(III) and P-O in $–PO_4^-$ of SSLB(-)
[GO-Cd]–SSLB(-)	-3412.431	-2793.321	-6205.960	-130.65	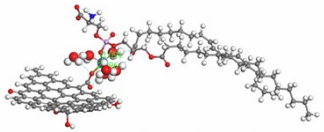	Coordination between Cd(II) and P-O in $–PO_4^-$ of SSLB(-)

Table S12 Binding energies for the adsorption of metals onto the SSLBs (kcal/mol).

SSLBs	Metals	Adsorption groups			
		Ester	Phosphate	Carboxyl	Amino
SSLB(+)	Fe(III)	-76.19	-	-	-
	Cu(II)	-65.23	-	-	-
	Ni(II)	-57.81	-	-	-
	Cd(II)	-54.10	-	-	-
SSLB(0)	Fe(III)	-37.16	-59.85	-	-
	Cu(II)	-28.85	-46.77	-	-
	Ni(II)	-25.38	-43.19	-	-
	Cd(II)	-23.93	-39.07	-	-
SSLB(−)	Fe(III)	-57.44	-65.55	-64.88	-52.86
	Cu(II)	-29.49	-55.56	-47.69	-19.41
	Ni(II)	-29.06	-51.67	-37.02	-18.11
	Cd(II)	-24.40	-45.72	-35.77	-17.84

Table S13 Binding energies for the co-attachment of GO and metals by SSLBs (kcal/mol)

	Metals	SSLB(+)	SSLB(0)	SSLB(-)
SSLBs–[GO-metal]	Fe(III)	-173.74	-141.56	-171.77
	Cu(II)	-154.45	-133.25	-147.97
	Ni(II)	-151.43	-131.44	-143.04
	Cd(II)	-151.12	-127.89	-139.17
[GO-metal]–SSLBs	Fe(III)	-168.59	-138.44	-153.14
	Cu(II)	-147.94	-131.17	-141.7
	Ni(II)	-144.57	-124.89	-131.98
	Cd(II)	-140.3	-124.82	-130.65

Table S14 Gaussian calculation results for interactions between GO, SSLB(0) and Cu(II).

Systems	Total energy (*E*, Hartree)				Binding energy (kcal/mol)	Structure	Binding site
	SSLB(0)	GO	Cu	After binding			
GO-SSLB(0)	-2722.509	-2785.666	–	-5508.223	-30.20	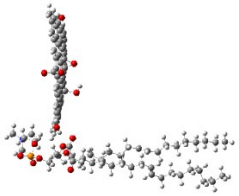	Hydrogen bonding between C−O of −COO− in SSLB(0) and −OH on the edge of GO
SSLB(0)-Cu(II)	-2722.509	–	-1944.823	-4667.435	-64.29	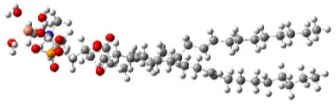	Coordination between Cu(II) and P-O of $–PO_4^-$ in SSLB(0)
GO-Cu(II)	–	-2785.666	-1944.823	-4730.926	-273.69	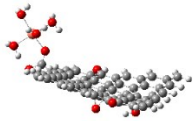	Coordination between Cu(II) and C−O of $−COO^−$ in GO
SSLB(0)–[GO-Cu(II)]	-2722.509	-2785.666	-1944.823	-7453.513	-322.65	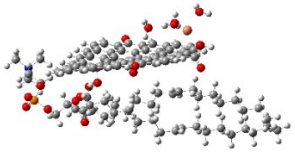	Hydrogen bonding between C−O of −COO− in SSLB(0) and −OH on the basal plane of GO
[GO-Cu(II)]–SSLB(0)	-2722.509	-2785.666	-1944.823	-7453.451	-284.04	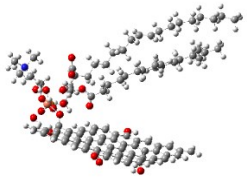	Coordination between Cu(II) and P-O in $–PO_4^-$ of SSLB(0)

Table S15 Gaussian calculation results for interactions between GO, SSLB(0) and Cu(II) with and without considering the van der Waals dispersions.

System	Total energy (E, Hartree)		ΔE (kcal/mol)
	Considering the van der Waals dispersions	Without considering the van der Waals dispersions	
GO-SSLB(0)	-5508.223	-5507.90	-202.69
SSLB(0)-Cu(II)	-4667.435	-4667.27	-103.54
GO-Cu(II)	-4730.926	-4730.75	-110.44
SSLB(0)–[GO-Cu]	-7453.513	-7453.07	-277.99
[GO-Cu]–SSLB(0)	-7453.451	-7453.18	-170.06

Table S16 HOMO and LUMO orbitals and energy levels of GO and GO-metals.

	(a) GO	(b) GO-Fe(III)	(c) GO-Cu(II)	(d) GO-Ni(II)	(e) GO-Cd(II)
HOMO (eV)	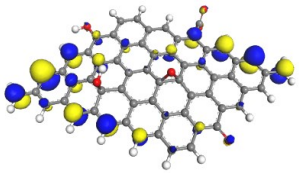	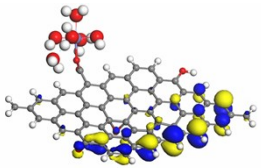	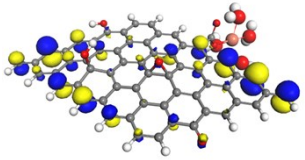	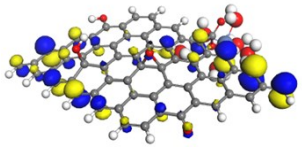	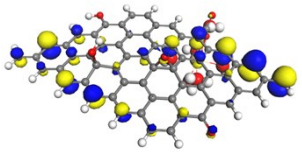
	-4.111	-4.610	-4.674	-4.501	-4.499
LUMO (ev)	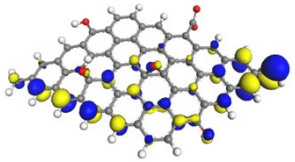	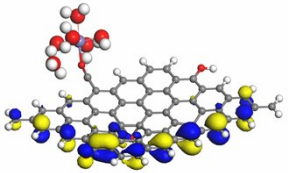	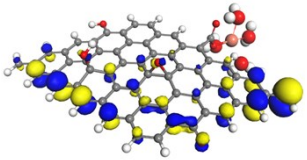	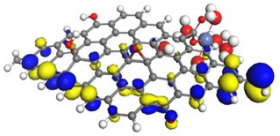	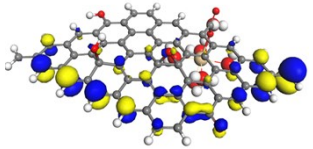
	-4.076	-4.366	-4.530	-4.384	-4.380

Table S17 Band shift of GO, SSLB (0), GO-Cu(II), SSLB(0)-GO, SSLB(0)-Cu(II) and SSLB(0)-GO-Cu(II) in XPS spectra.

Position (eV)	C 1s				O 1s			P 2p	Cu 2p		
	C-C	C-O	C=O	O-C=O	O-C=O	C-O	C-OH/ P-O-C	-	Cu $2p_{1/2}$	Cu^{2+}	Cu $2p_{3/2}$
GO	284.8	286.7	287.9	288.8	531.7	532.5	533.2	-	-	-	-
SSLB(0)	284.8	286.7	-	288.8	531.7	532.4	533.1	133.6	-	-	-
GO-Cu(II)	284.8	286.9	287.9	288.8	531.8	532.6	533.3	-	934.5	944.5	954.5
SSLB(0)-GO	284.8	287.0	287.9	288.8	532.1	532.8	533.5	133.7	-	-	-
SSLB(0)-Cu(II)	284.8	286.8	-	288.9	531.9	532.6	533.3	133.8	933.5	943.5	953.5
SSLB(0)-GO-Cu(II)	284.8	287.0	287.9	288.8	532.0	532.8	533.5	134.0	934.3	941.3	954.3

References

1 J. M. Luo, X. B. Luo, J. Crittenden, J. H. Qu, Y. H. Bai, Y. Peng and J. H. Li, Removal of antimonite (Sb(III)) and antimonate (Sb(V)) from aqueous solution using carbon nanofibers that are decorated with zirconium oxide (ZrO_2), *Environ. Sci. Technol.*, 2015, **49**, 11115-11124.

2 S. Li, F. Wang, W. Pan, X. Yang, Q. Gao, W. Sun and J. Ni, Molecular insights into the effects of Cu(II) on sulfamethoxazole and 17β-estradiol adsorption by carbon nanotubes/CoFe2O4 composites, *Chem. Eng. J.*, 2019, **373**, 995-1002.

3 G. Y. Yuan, Y. Tian, J. Liu, H. Tu, J. L. Liao, J. J. Yang, Y. Y. Yang, D. Q. Wang and N. Liu, Schiff base anchored on metal-organic framework for Co (II) removal from aqueous solution, *Chem. Eng. J.*, 2017, **326**, 691-699.

4 K. Yang, B. Chen, X. Zhu and B. Xing, Aggregation, adsorption, and morphological transformation of graphene oxide in aqueous solutions containing different metal cations, *Environ. Sci. Technol.*, 2016, **50**, 11066-11075.

5 X. Ren, Q. Wu, H. Xu, D. Shao, X. Tan, W. Shi, C. Chen, J. Li, Z. Chai, T. Hayat and X. Wang, New insight into GO, cadmium(II), phosphate interaction and its role in GO colloidal behavior, *Environ. Sci. Technol.*, 2016, **50**, 9361-9369.

6 S. Yang, C. Chen, Y. Chen, J. Li, D. Wang, X. Wang and W. Hu, Competitive adsorption of PbII, NiII, and SrII ions on graphene oxides: A combined experimental and theoretical study, *ChemPlusChem*, 2015, **80**, 480-484.

7 C. Z. Wang, J. H. Lan, Q. Y. Wu, Y. L. Zhao, X. K. Wang, Z. F. Chai and W. Q. Shi, Density functional theory investigations of the trivalent lanthanide and actinide extraction complexes with diglycolamides, *Dalton T.*, 2014, **43**, 8713-8720.

8 E. V. Basiuk, L. Huerta and V. A. Basiuk, Noncovalent bonding of 3d metal(II) phthalocyanines with single-walled carbon nanotubes: A combined DFT and XPS study, *Appl. Surf. Sci.*, 2019, **470**, 622-630.

9 R. Sitko, E. Turek, B. Zawisza, E. Malicka, E. Talik, J. Heimann, A. Gagor, B. Feist and R. Wrzalik, Adsorption of divalent metal ions from aqueous solutions using graphene oxide, *Dalton Trans.*, 2013, **42**, 5682-5689.

10 D. Gu and J. B. Fein, Adsorption of metals onto graphene oxide: Surface complexation modeling and linear free energy relationships, *Colloids Surf. A Physicochem. Eng. Asp.*, 2015, **481**, 319-327.

11 W. Peng, H. Li, Y. Liu and S. Song, A review on heavy metal ions adsorption from water by graphene oxide and its composites, *J. Mol. Liq.*, 2017, 230, 496-504.

12 K. Yang, B. Chen, X. Zhu and B. Xing, Aggregation, adsorption, and morphological transformation of graphene oxide in aqueous solutions containing different metal cations, *Environ. Sci. Technol.*, 2016, **50**, 11066-11075.

13 A. S. Dobrota, I. A. Pašti and N. V. Skorodumova, Oxidized graphene as an

electrode material for rechargeable metal-ion batteries – a DFT point of view, *Electrochim. Acta*, 2015, **176**, 1092-1099.

14 S. Yu, X. Wang, Y. Ai, Y. Liang, Y. Ji, J. Li, T. Hayat, A. Alsaedi and X. Wang, Spectroscopic and theoretical studies on the counterion effect of Cu(ii) ion and graphene oxide interaction with titanium dioxide, *Environ. Sci.: Nano*, 2016, **3**, 1361-1368.

15 X. Wang, Z. Chen and S. Yang, Application of graphene oxides for the removal of Pb(II) ions from aqueous solutions: Experimental and DFT calculation, *J. Mol. Liq.*, 2015, **211**, 957-964.

16 J. Wei, W. Zhang, W. Pan, C. Li and W. L. Sun, Experimental and theoretical investigations on Se(iv) and Se(vi) adsorption to UiO-66-based metal–organic frameworks, *Environ. Sci.: Nano*, 2018, **5**, 1441-1453.

17 J. Wei, W. L. Sun, W. Pan, X. Yu, G. Sun and H. Jiang, Comparing the effects of different oxygen-containing functional groups on sulfonamides adsorption by carbon nanotubes: Experiments and theoretical calculation, *Chem. Eng. J.*, 2017, **312**, 167-179.

18 W. L. Sun, J. Xia and Y.-C. Shan, Comparison kinetics studies of Cu(II) adsorption by multi-walled carbon nanotubes in homo and heterogeneous systems: Effect of nano-SiO2, *Chem. Eng. J.*, 2014, **250**, 119-127.

19 W. L. Sun, K. Yin and X. Yu, Effect of natural aquatic colloids on Cu(II) and Pb(II) adsorption by Al_2O_3 nanoparticles, *Chem. Eng. J.*, 2013, **225**, 464-473.

20 I. F. Amaral, P. L. Granja and M. A. Barbosa, Chemical modification of chitosan by phosphorylation: an XPS, FT-IR and SEM study, *J. Biomat. Sci.-Polym. E*, 2012, **16**, 1575-1593.

21 L. Wang, S. C. B. Gopinath, P. Anbu, R. D. A. A. Rajapaksha, P. Velusamy, K. Pandian, M. K. M. Arshad, T. Lakshmipriya and C.-G. Lee, Photovoltaic and antimicrobial potentials of electrodeposited copper nanoparticle, *BioChem. Eng. J.*, 2019, **142**, 97-104.

22 Y.-J. Kim and K.-S. Ryu, The surface-modified effects of Zn anode with CuO in Zn-air batteries, *Appl. Surf. Sci.*, 2019, **480**, 912-922.

23 S. J. Ding, Q. Q. Zhang, D. W. Zhang, J. T. Wang and W. W. Lee, Copper metallization of low-dielectric-constant a-SiCOF films for ULSI interconnects, *J. Phys-Condens. Mat.*, 2001, **13**, 6595-6608.

24 W. L. Sun, C. Wang, W. Pan, S. Li and B. Chen, Effects of natural minerals on the adsorption of 17β-estradiol and bisphenol A on graphene oxide and reduced graphene oxide, *Environ. Sci.: Nano*, 2017, **4**, 1377-1388.

25 W. L. Sun, M. Li, W. Zhang, J. Wei, B. Chen and C. Wang, Sediments inhibit adsorption of 17β-estradiol and 17α-ethinylestradiol to carbon nanotubes and graphene oxide, *Environ. Sci.: Nano*, 2017, **4**, 1900-1910.

26 M. B. Hay and S. C. B. Myneni, Structural environments of carboxyl groups in natural organic molecules from terrestrial systems. Part 1: Infrared spectroscopy, *Geochim. Cosmochim. Acta*, 2007, **71**, 3518-3532.

27 L. Landström, L. Örebrand, K. Svensson and P. O. Andersson, Spectroscopic investigation of substrates contaminated by chemical warfare agents, *J. Anal. Atom. Spectrom.*, 2015, **30**, 2394-2402.
28 W. Yan, L. Yan, J. Duan and C. Jing, Sorption of organophosphate esters by carbon nanotubes, *J. Hazard. Mater.*, 2014, **273**, 53-60.
29 L. Xiong, Y. Yang, J. Mai, W. Sun, C. Zhang, D. Wei, Q. Chen and J. Ni, Adsorption behavior of methylene blue onto titanate nanotubes, *Chem. Eng. J.*, 2010, **156**, 313-320.
30 P. Trivedi, L. Axe and J. Dyer, Adsorption of metal ions onto goethite: single-adsorbate and competitive systems, *Colloids Surf. A*, 2001, **191**, 107-121.
31 T. B. Kinraide and U. Yermiyahu, A scale of metal ion binding strengths correlating with ionic charge, Pauling electronegativity, toxicity, and other physiological effects, *J. Inorg. Biochem.*, 2007, **101**, 1201-1213.
32 S. Mustafa, M. Irshad, M. Waseem, K. H. Shah, U. Rashid and W. Rehman, Adsorption of heavy metal ions in ternary systems onto Fe(OH)3, *Korean J. Chem. Eng.*, 2013, **30**, 2235-2240.
33 Y. Gao, X. Ren, J. Wu, T. Hayat, A. Alsaedi, C. Cheng and C. Chen, Graphene oxide interactions with co-existing heavy metal cations: adsorption, colloidal properties and joint toxicity, *Environ. Sci.: Nano*, 2018, **5**, 362-371.
34 http://phases.imet-db.ru/elements/main.aspx